

# 1 Future heat extremes likely to have been underestimated

2  
3 N. Freychet<sup>1</sup>, G. Hegerl<sup>1</sup>, D. Mitchell<sup>2</sup>, M. Collins<sup>3</sup>

4  
5 <sup>1</sup>*School of Geosciences, University of Edinburgh, Edinburgh, UK*

6 <sup>2</sup>*School of Geographical Sciences, University of Bristol, Bristol, UK*

7 <sup>3</sup>*College of Engineering, Mathematics and Physical Sciences, University of Exeter,*  
8 *Exeter, UK*

9  
10 **In a warming world, temperature extremes are expected to show a distinguishable**  
11 **change over much of the globe<sup>1</sup> and in many regions this change has already**  
12 **been detected in observations<sup>2,3</sup>. Although previous studies predict an increase in**  
13 **heat extreme events, the magnitude of the change varies greatly among different**  
14 **models even for the same mean warming<sup>4</sup>. This uncertainty has been linked to**  
15 **differences in land-atmosphere feedbacks across models<sup>2</sup>. Here we show that a**  
16 **significant constraint for future projections can be based on the ability of climate**  
17 **models to accurately simulate the variability of daily atmospheric surface**  
18 **maximum temperature (TX). By applying an emergent constraint (EC) locally on a**  
19 **metric describing TX variability with a large ensemble of CMIP5<sup>5</sup> and CMIP6<sup>6</sup>**  
20 **models we demonstrate that the best estimate increase in hot extremes could be**  
21 **worse than previously estimated over a large part of the land, with an increase in**

22 **extremes of up to 50% larger than based on the multi-model mean. Our findings**  
23 **highlight the importance to correctly simulate TX variability during the historical**  
24 **period. Analysis of models soil moisture suggests that the EC arises because**  
25 **both TX variability and changes in hot extremes are related to land surface**  
26 **humidity processes.**

27

28 Temperature extremes impact strongly on society and can have negative consequences  
29 on health<sup>7</sup>, agriculture<sup>8</sup> or water resources<sup>9</sup>. Daily maximum temperature (TX) is often  
30 used to measure heat wave intensity. It is governed by many processes, including  
31 accumulation of solar radiation, heat transport, and sensible and latent heat flux  
32 exchange with the surface. Particularly, energy used to evaporate surface moisture can  
33 limit atmospheric warming and thus TX<sup>10</sup>. At any given location TX tends to be larger  
34 under drier surface conditions than wetter conditions. Another way to formulate this idea  
35 is that soil moisture (and other surface humidity variables) deficit can lead to amplified  
36 TX (and with it, potentially amplified heat waves). There is evidence that many current  
37 climate models dry too much<sup>11</sup> and we hypothesize that this amplifies TX variability (thus  
38 heat wave frequency<sup>12</sup>) whereas more accurate models may see this amplification in the  
39 upcoming decades. We postulate that this could lead to large differences between  
40 models in terms of heat wave changes under climate warming.

41

42 Many indices of TX can be used to describe hot events (as defined by Expert Team on  
43 Climate Change Detection and Indices, ETCCDI). We chose a simple derived index that

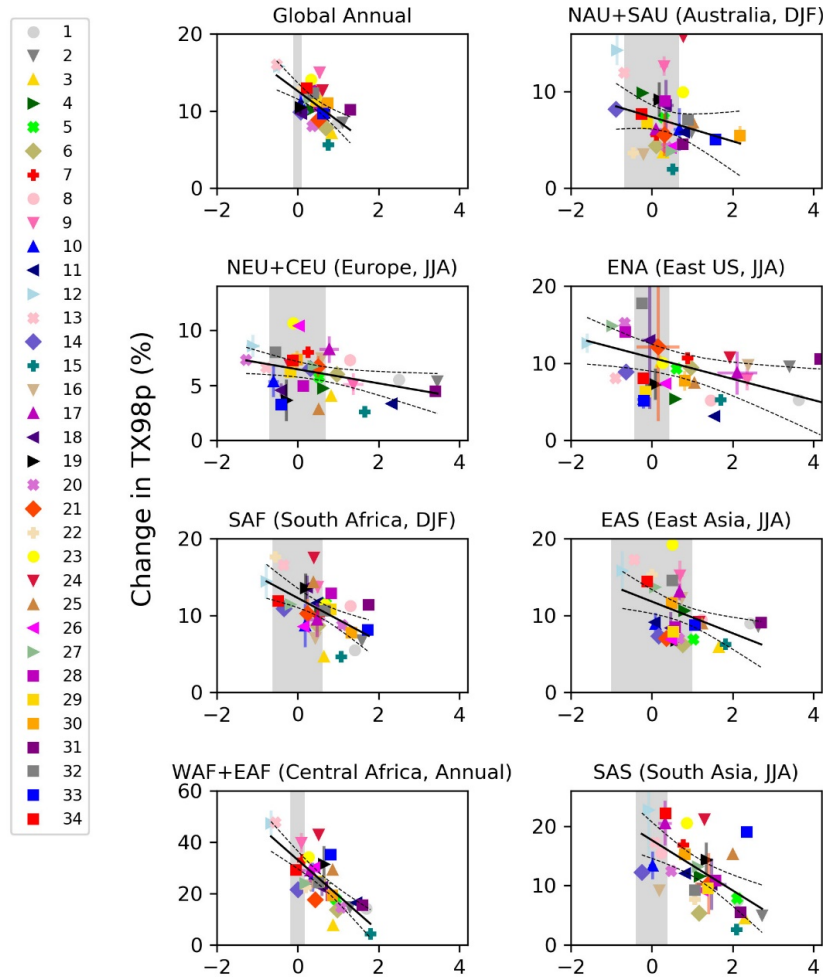
44 can be applied easily at global scale, namely the number of days above the 98<sup>th</sup>  
45 percentile (TX98p, see methods for detailed computation). We only focus on the  
46 warmest season (June to August for North Hemisphere, December to February for  
47 South Hemisphere and all year for the 15°S-15°N tropical area). TX98p indicates for  
48 each location when a day is considered as extremely hot (relative to the daily  
49 climatology of TX at this location). By definition, it represents the 2% hottest days during  
50 the baseline period (1995-2005) at each location, and we evaluate its change in climate  
51 projections (see methods for details). We also define a metric to quantify the historical  
52 variability of TX at each location,  $\Delta TX$ . This metric indicates at each grid point and for  
53 each calendar day the distance between mean TX and the 95<sup>th</sup> percentile of TX (TX95p)  
54 in degrees C.  $\Delta TX$  gives an indication of the temperature difference between a hot day  
55 compared to the climatology. It is used to evaluate models against a reference dataset,  
56 ERA5 reanalysis<sup>13</sup>. This difference has been found to be too high in some climate  
57 models (e.g. 14). Computation of  $\Delta TX$  implies that we ignore any bias in the mean TX of  
58 a model (compared to ERA5) and focus only on TX variability. Note that our results are  
59 not sensitive to using another threshold for heat wave index, e.g. the 95<sup>th</sup> percentile  
60 instead of 98<sup>th</sup> percentile (displayed in supplementary information).

61

62 Previous studies have shown that soil moisture deficits enhance surface temperature  
63 extremes<sup>15,16</sup> and have a strong impact on severe events such as heat waves<sup>17</sup>. Here we  
64 focus on daily timescale temperatures and due to limited availability of humidity model  
65 outputs at high temporal resolution (especially evaporation and integrated soil moisture  
66 are not available at daily timescales for CMIP5 outputs) we use the upper layer of soil

67 moisture (called USM in model data, here referred to as Upper layer Soil Moisture USM  
68 for simplicity) as an indicator of land-atmosphere humidity interaction. Although USM is  
69 controlled by several factors such as infiltration, horizontal transport and evaporation  
70 (with parametrisation varying with land surface models), we assume it can be an  
71 indicator of land surface conditions during hot days. We verified that USM conditions  
72 during days above the 98<sup>th</sup> percentile exhibit a negative correlation with  $\Delta TX$  over 80%  
73 of the land (Fig.S1,a), i.e. models with highest  $\Delta TX$  are also drying the most. This  
74 confirms the relationship between surface humidity and TX variability during the  
75 baseline period. For some regions this relationship is not or poorly verified. This may be  
76 due to other variables influencing humidity and not included in our analysis (e.g.  
77 vegetation, deeper layer soil moisture or irrigation), specific land properties (such as  
78 permafrost for northern regions) or simply because the number of individual models for  
79 this analysis is limited. Thus even if we consider hereafter  $\Delta TX$  as an indicator of model  
80 historical performances in surface humidity feedback, the physics of the relationship  
81 could be closer explored in each model.

82



83

Difference in TX variability ( $\Delta$ TX) between models and ERA5 ( $^{\circ}$  C)

84 Fig.1: Relationship between  $\Delta$ TX and projected change in TX98p in selected regions

85 The figure shows for each CMIP5 and CMIP6 models the change in the ensemble average frequency of  
 86 hot days (TX98p, y-axis, in % of days) in the future (last decade of rcp45 and ssp245) compared to the  
 87 present period (1995-2005) plotted against the a variability metric for daily maximum temperature ( $\Delta$ TX)  
 88 during the historical period (x-axis, in  $^{\circ}$ C) averaged over different sub-regions.  $\Delta$ TX measures the  
 89 difference between daily TX95p and mean TX in a model compared to that observed. Solid black line is  
 90 the linear regression between  $\Delta$ TX and TX98p, and dashed black lines show the 95% confidence interval.  
 91 Grey shading represents  $\Delta$ TX uncertainties estimated from HAPPI ensemble. Acronyms refer to AR5  
 92 region definitions and numbers refer to models in Table 1.

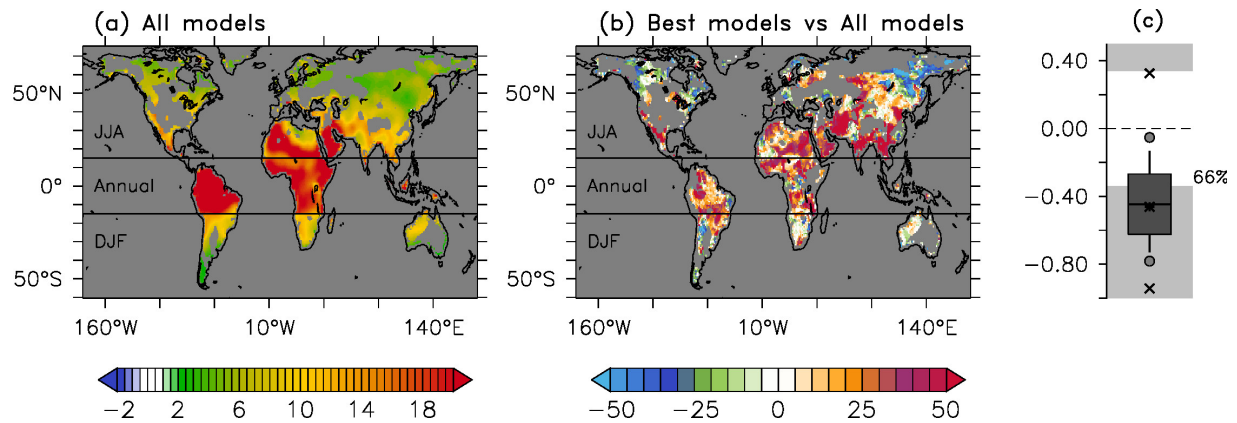
93

94 We also verify that  $\Delta TX$  is strongly correlated to TX98p change for different warming  
95 targets. Over most of land the relationship between  $\Delta TX$  and TX98p change is negative  
96 (Fig.1) and significant (Fig.S2), indicating that in regions with overestimated variance for  
97 hot days the future change in TX98p is smaller on average. Thus, this simple metric is  
98 justified to constrain model projections. In the following we mask results only where  
99  $\Delta TX$ -TX98p correlation is significant. It is the case at global scale (figure 1), where the  
100 metric indicates a tendency to too large  $\Delta TX$  for most models, and over most of regions  
101 except central North America, central Europe and northern polar regions.

102

103 The EC methodology requires understanding and accounting for observational and  
104 model variability and uncertainties so they it can decide how consistent they are<sup>18</sup>. We  
105 use the internal variability of a large multi-member historical ensembles (HAPPI) that  
106 was forced with observed sea surface temperatures to estimate  $\Delta TX$  variability at each  
107 location. We then consider this information as an uncertainty range for  $\Delta TX$  based on  
108 ERA5 and to evaluate when models fit within this range (with multi-member models  
109 having narrower uncertainty, see methods).

110



112 Fig2: **Implication of emergent constraint for future change in extremes**

113 (a) Ensemble mean (all CMIP models) difference in TX98p per degree warming compared to the baseline  
 114 1995-2005 period, expressed as a percentage of days (+X% means an extra X% of days each year will  
 115 be above the 98<sup>th</sup> percentile, see methods). (b) Difference in TX98p projections between models that  
 116 reproduce the observed constraint and all models, expressed as a percentage of the change in (a). (a)  
 117 and (b) display results only where the correlation between TX98p and  $\Delta TX$  is significant (see  
 118 supplementary Fig.S2). (c) Box plot distribution of cross-models correlation coefficients between historical  
 119  $\Delta TX$  and change in TX98p computed at each grid point. Dark grey box is the 25-75 interquartile, with  
 120 horizontal bar inside being the median; vertical solid black line shows the 10-90 interquartile; lower and  
 121 upper circle symbols are percentile 5 and 95 respectively; lower and upper cross symbols are percentile 1  
 122 and 99 respectively. Black cross in the box is the mean. Only values in light grey shading are significant at  
 123 the 95% confidence level. The percentage written indicate how many grid points are above this  
 124 confidence level.

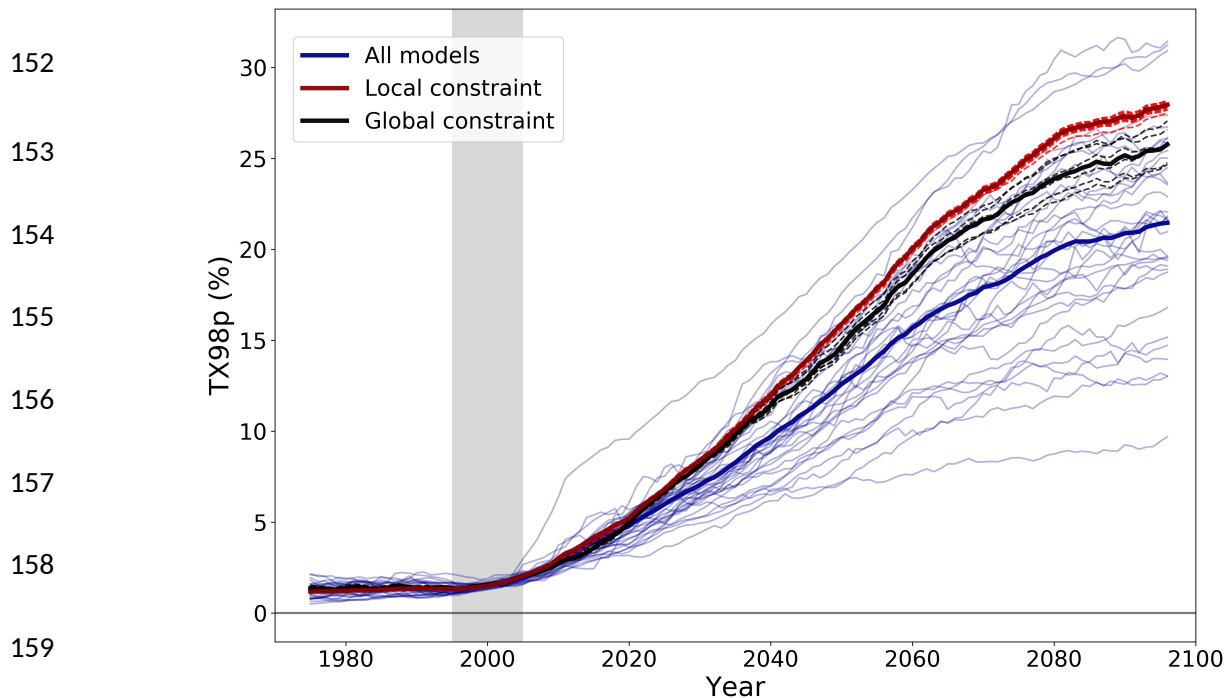
125

126 Using  $\Delta TX$  to constrain climate projections by selecting in each gridbox (after spatial  
 127 smoothing, see methods) the models within the observed constraint, we found that  
 128 changes in TX98p are larger than estimated by an unconstrained ensemble over a large

129 part of the land (Fig.2). Africa, South and Central Asia and South America have a  
130 particularly strong signal, locally above 50% increase in the number of exceedances of  
131 the 98<sup>th</sup> percentile (although the magnitude of the difference may be partly explained by  
132 the number of selected models at each location); i.e. twice as many hot days as in  
133 unconstrained predictions. This means models representing more accurately  $\Delta TX$   
134 during baseline period (and hypothetically humidity feedbacks) tend to warm faster  
135 compared to the other models. Similar relationships are found for all climate warming  
136 targets (supplementary Fig.S11 and S12), although the area with significant correlation  
137 is reduced for 1.5°C target. This influence of our EC persists through different warming  
138 targets and is confirmed robust by several sensitivity tests (see methods).

139 Applying an EC based on global mean  $\Delta TX$  (i.e. selecting or rejecting a single model on  
140 a global mean relationship) leads to slightly weaker, but still valid, amplification (Fig.3).  
141 Using a regional constraint to select the best models at each location seems more  
142 appropriate, as no model is considered good everywhere (supplementary Fig.S3). The  
143 constrained TX98p signal (either by local or global method) suggest that the level of  
144 increase previously estimated by the end of the century could be reached by 2060  
145 instead, i.e. 40 years earlier. All these results are verified independent of model  
146 selection by performing sensitivity tests where one model is removed randomly from the  
147 ensemble (Fig.3). The regional constraints results remain highly consistent. The global  
148 constraint is still consistent but slightly more sensitive to model selection (due to the  
149 small size of this ensemble that fall near the uncertainty range). Thus using regional  
150 constrain method here leads to more stable and reliable results.





160 Fig.3: **Global evolution of hot extremes in unconstrained and constrained ensembles.**

161 Timeseries of global mean TX98p (%) for the mean (thick solid line) of all CMIP5 and CMIP6 models  
 162 (blue) and constrained models with constraint applied to each significant grid point (red). Ensemble  
 163 means are computed, each year, for each grid point from a 9-years running mean of TX98p, then globally  
 164 averaged to obtain a global mean value. This method allows a more detailed computation of constrained  
 165 ensemble, as the number of models varies from one region to another. Thin blue lines indicate individual  
 166 model results. Solid back line shows the mean of a sub-ensemble (7 models) where EC is based on  
 167 globally averaged  $\Delta TX$  (instead of applying EC at each grid point). Gray shading highlights the baseline  
 168 period to compute the TX98p threshold. Red (and black) dashed lines show a sensitivity study where one  
 169 model is removed before computation of local (and global) constrained ensemble mean (test repeated for  
 170 each model of each ensemble). For each model, TX98p is linearly scaled by comparing its individual  
 171 change in  $T_{as}$  to the ensemble mean change in  $T_{as}$ .

172

173 An important point is to verify the physical mechanism linking change in TX98p and land  
 174 drying, although due to limited data we only use monthly timescale USM outputs (i.e.

175 mean land drying, not specifically during hot days). The relationship between change in  
176 TX98p and mean USM is overall negative, indicating larger temperature variability for  
177 drier soils, and supporting our hypothesis (supplement material Fig.S1,b), although it is  
178 significant only over few areas and not necessarily where EC signal is the strongest  
179 (especially, it is weak over the tropical area). This may be explained by several reasons.  
180 First, USM is only one part of land moisture and does not include vegetation (which can  
181 be an important factor moderating humidity over tropical land). Secondly due the limit of  
182 USM model output data to monthly we may not capture the specific heat event well  
183 enough, making the statistical relationship more difficult to estimate. Third, a full daily  
184 analysis on evaporation, vegetation and soil moisture structure would be needed to  
185 understand how these processes changes under very specific conditions (hot days).  
186 This is obviously a strong limit to our current understanding and we can only raise a  
187 physical hypothesis. We stress here the importance of high temporal resolution surface  
188 humidity outputs to fully understand extreme event processes and humidity feedbacks.

189 We note that over some regions constrained models do not indicate an increase in  
190 TX98p, especially over northern part of America and Siberia. These correspond to areas  
191 with weak correlation between  $\Delta TX$  and TX98p. Other processes may be more  
192 dominant in these regions, and drying of soil may be not a factor in high latitudes.  
193 Additionally, permafrost land-atmosphere exchanges and humidity processes are  
194 different there.

195 Overall, our results indicate that climatological bias in the difference between hot and  
196 average days in climate models lay lead to an underestimate of the frequency of  
197 unusually hot days in the future.

198

199

200 **Acknowledgment**

201 We acknowledge the E-OBS dataset from the EU-FP6 project UERRA  
202 (<http://www.uerra.eu>) and the Copernicus Climate Change Service, and the data  
203 providers in the ECA&D project (<https://www.ecad.eu>). This research used science  
204 gateway resources of the National Energy Research Scientific Computing Center, a  
205 DOE Office of Science User Facility supported by the Office of Science of the U.S.  
206 Department of Energy under Contract No.DE-AC02-05CH11231. This research is  
207 funded by NERC grant award NE/S004661/1 EMERGENCE project.

208

209

210

211

212

## 213 **METHOD**

### 214 **Definition and computation of indices**

215 Our analysis focusses on daily maximum temperature (TX) extremes (TX98p). We  
216 define TX98p as the number of days above the daily climatological 98<sup>th</sup> percentile. The  
217 latter is computed for each location and each calendar day by pulling together all days  
218 within +/- 15 days window of this calendar day during the 1995-2005 period and  
219 selecting the 2% highest values.

220 We also define a metric,  $\Delta TX$ , to evaluate the variability of TX during the baseline  
221 period. It is done by first calculating the mean and 95<sup>th</sup> percentile of the temperature  
222 distribution for each calendar day at each location (by pulling 15 days around each  
223 calendar day together as for 98<sup>th</sup> percentile describe above). The distance between the  
224 95<sup>th</sup> percentile and the mean gives an indication of TX variability for each day and each  
225 location. It is computed for each model ( $\Delta TX_{\text{model}}$ ) and for the reference dataset ( $\Delta TX_{\text{ref}}$ ;  
226 the ERA5 reanalysis) and the difference between the two defines our metric:  $\Delta TX =$   
227  $\Delta TX_{\text{model}} - \Delta TX_{\text{ref}}$ . We only focus on the warm season, when hot extreme are likely to  
228 happen (June-August for North Hemisphere, December-February for South Hemisphere  
229 and all year for the 15°S-15°N tropical area). Positive values mean a model over-  
230 estimates the TX variability compared to the reference (i.e. it tends to warm up too  
231 quickly and over-estimated high values of TX), negative values indicate an  
232 underestimate. For the metric, we choose the 95<sup>th</sup> percentile to ensure reasonably good  
233 sampling of the variability across the base period (as it is used to constrain models)  
234 while for future changes we focus on the 98<sup>th</sup> percentile which correspond to more  
235 extreme values. We verified that EC results are not very sensitive to the choice of

236 threshold by doing a sensitivity test using the 95<sup>th</sup> percentile as threshold instead 98<sup>th</sup>  
237 (supplementary Fig.S4).

238 Each index is computed individually for each model (and eventually each member) on  
239 their native grid. Results are then interpolated on a common 1° grid before being  
240 averaged across all models. As temperature extremes are relatively large-scale, and  
241 grids vary only between 1 and 2.5 degrees latitude/longitude across models, results are  
242 not sensitive to the order of operation.

243

## 244 **Datasets**

### 245 *- CMIP models*

246 An ensemble of 27 individual models from CMIP5<sup>5</sup> and 7 from CMIP6<sup>6</sup> is used. Some  
247 only have a single member available while some provide a multi-members ensemble. In  
248 the latter case, multi-member results are always computed individually and then  
249 averaged to provide one mean result for a single model. We consider a reference period  
250 as the historical 1995-2005 decade (being the last decade of CMIP5 historical forcing).  
251 Climate projections are investigated using the RCP4.5<sup>19</sup> and SSP245<sup>20</sup> pathways for  
252 CMIP5 and CMIP6 models respectively. Both scenarios are expected to be close,  
253 although each model leads to different mean temperature increases (Fig.S5).

254 Three climate projection targets are considered:

255 - *end-of-century*, by selecting the 2091-2100 decade for each model.

256 - *+1.5°C and +2°C warming above pre-industrial mean*. For these two, we follow a

257 similar approach as in 21 and select for each member of each model the first decade  
258 when the average atmospheric surface temperature ( $T_{as}$ ) of each year of the decade is  
259 above the corresponding threshold (Fig.S5). As we use 1995-2005 as a baseline, the  
260 actual threshold (relative to the baseline) is chosen as  $+0.7^{\circ}\text{C}$  and  $+1.2^{\circ}\text{C}$  for targets  
261  $+1.5^{\circ}\text{C}$  and  $+2^{\circ}\text{C}$  above pre-industrial respectively, as in the HAPPI experiment  
262 design<sup>22</sup>. Although the exact definition of these levels can be sensitive<sup>23</sup>, for this work  
263 the main point is that each model or member should reach a similar magnitude of  
264 warming. A few members and models do not meet the condition for the  $+2^{\circ}\text{C}$  target  
265 before the end of the century. For these cases, we select instead the last projection  
266 decade 2091-2100. If the mean increase in  $T_{as}$  over this decade is above the threshold  
267 ( $+1.2^{\circ}\text{C}$ ) then we keep the model or member. Otherwise we do not include it in the  
268 analysis for this projection target. This leads us to discard 4 members.

269 For each climate projection target, results of each member or model are normalised by  
270 their respective mean change over the decade (relative to our baseline) in  $T_{as}$  (and then  
271 averaged to provide ensemble mean results). Thus, no matter the target projection all  
272 results are shown for  $+1\text{C}$  warming above the baseline. We tested the sensibility of the  
273 results by using raw results (without normalisation) for each model but both methods  
274 lead to very close results in terms of EC amplification (Fig.3 and Fig.S6), although raw  
275 results have larger uncertainties. Thus, we largely focus on normalised results in the  
276 body of the paper.

277 For most of the models we could get daily TX data for both historical and projection  
278 periods. Daily soil moisture data are more limited (9 CMIP5 and 5 CMIP6 models).  
279 Supplementary Table 1 provides details about outputs used for each variable.

280

281 - HAPPI ensemble and  $\Delta TX$  uncertainty

282 To evaluate the uncertainties on  $\Delta TX$  during the baseline period we use several  
283 atmospheric models from the HAPPI ensemble<sup>22</sup>. Each model provides daily output for  
284 the 1995-2005 decade. We select 5 models with a hundred or more members and  
285 compute  $\Delta TX$  for each member (same method as for CMIP models). Then, using  
286 internal variability of each model (multi-members ensemble standard deviation,  $\sigma$ ), we  
287 estimate  $\Delta TX$  uncertainties for each location and calendar day (Fig.S7). One model has  
288 a mean bias that is much larger than other models (CanAM4), we thus exclude it. For  
289 other models, the  $\Delta TX$  internal variability is consistent, so we use the mean of four  
290 remaining model variabilities (i.e. averaging the four internal STD) as a measure of  $\Delta TX$   
291 uncertainties ( $\sigma_{\text{HAPPI}}$ ).

292 The sensitivity of this choice is also tested by using individual model STD instead of  
293 ensemble mean (Fig.S8). It shows that results stay consistent for each case. We note  
294 that the uncertainty so described is that of atmospheric variability only. However, both  
295 the HAPPI ensemble and the ERA5 reanalysis are driven by the same SSTs hence this  
296 choice is conservative to characterize observational uncertainty.

297 Internal variability in the climate models used is reduced by ensemble averaging. To  
298 take into account the specific number of members for each individual model, the  
299 uncertainty between OBS and models is expressed as:  $(\sigma_{\text{HAPPI}}^2 + (\sigma_{\text{HAPPI}}^2 / N))^{1/2}$  with N  
300 the number of members of a model. When the absolute value of  $\Delta TX$  fits within that

301 range then a model (eventually the multi-members ensemble mean) is considered as  
302 consistent with OBS.

303

304 - ERA5

305 The ERA5 reanalysis<sup>13</sup> is available for the full satellite observation period (1979-  
306 present). It provides hourly timescales data at 0.25° resolution on a reduced Gaussian  
307 grid, from which we computed daily TX for the 1995-2005 period.

308 We evaluated the variability of TX in ERA5 against two dense regional observational  
309 datasets (Fig.S9): A network of 756 homogenised station measurements for China,  
310 provided by the Chinese Meteorological Administration<sup>24</sup>; And gridded 0.25° E-OBS  
311 v19.0 dataset for Europe<sup>25</sup>. Chinese observations are first gridded on the same regular  
312 grid as ERA5 by linear interpolation.

313 Although the TX variability tends to be weaker in ERA5 than in observations, differences  
314 are within the range of uncertainties estimated from the HAPPI ensemble variability  
315 (Fig.S7) for both regions, hence we consider ERA5 sufficient.

316

### 317 **Emergent constraint (EC) method**

318 To decrease model projection uncertainties on TX98p, we use an EC method with  $\Delta TX$   
319 as a predictor (i.e. selecting models that are able to reproduce the width of the daily  
320 maximum temperature distribution TX, indicated by the distance between the 95<sup>th</sup>  
321 percentile and the median) and select those for prediction. To do this, CMIP models are



322 evaluated against ERA5 during the 1995-2005 period, and agree with it within  
323 atmospheric internal variability. We use variability from the HAPPI ensemble to  
324 characterize this uncertainty for better sampling. Models (ensemble mean in case of  
325 multi-members model) within the range of 2 times STD (i.e. the 95% confidence  
326 interval) are considered as reasonably realistic and selected for use in the constrained  
327 climate projections. Comparing constrained against unconstrained ensemble projections  
328 provides an estimate of the potential current bias in climate forecasts.

329 Constraints can arise from global or regional processes<sup>18</sup>. Here we use a regional  
330 constraint to take advantage of model information everywhere. We first apply a spatial  
331 smoothing of 5 degrees on  $\Delta TX$  over land (to improve sampling and avoid spatial  
332 discontinuity) then select the models that comply with the constraint within uncertainty at  
333 each grid point. Over most of the regions, the number of selected models is between 5  
334 and 10, except in central Africa where it is below 5. This is mainly due to very narrow  
335 observational variability over this region (Fig.S3 and S7). Most of models contribute to  
336 the projection over some part of land. Applying EC at a global scale instead (Fig.3 and  
337 S10) leads to similar patterns with slightly weaker amplification.

338 We also tested the sensitivity of EC results with different choices of uncertainty around  
339 the observational distribution with and different spatial smoothing (Fig.S8). Using  
340 narrower (wider) range of variability leads to slightly different results with less (more)  
341 models selected, corresponding to a noisier but more intense (smoother but less  
342 intense) signal. However, global patterns are still consistent with main results. Weaker  
343 spatial smoothing (3 degrees) leads to slightly noisier results while using too large  
344 smoothing (11 degrees) leads to large masked area (because we use only land grid

345 points or alternatively to large variation in actual applied smoothing). Thus 5 degrees  
346 smoothing is a good compromise.

347 Following recommendations from Hall et al., 2019, we first confirm the strong statistical  
348 relationship between  $\Delta TX$  and TX98p (Fig.1 and supplement S2). We then use a  
349 resampling method (by removing randomly a model from the ensemble) to test the  
350 robustness of the constraint (Fig.3). Finally, the physical mechanism hypothesis linking  
351 soil moisture,  $\Delta TX$  and TX98p is evaluated (Fig.S1), although this evaluation is  
352 somewhat limited due to limited soil moisture availability.

353

354

### 355 **Data availability**

356 The authors declare that all data that support the findings in the main article are  
357 available. All model data are publicly accessible via the Earth System Grid Federation node  
358 (<https://esgf-node.ipsl.upmc.fr/>). ERA5 data can be downloaded from ECMWF website  
359 (<https://www.ecmwf.int/en/forecasts/datasets/reanalysis-datasets/era5>). Scripts used to generate the  
360 main results will be made available on the University of Edinburgh datashare. All other data and code  
361 that support the figures in the [Supplementary Information](#) are available from the corresponding author  
362 on request.

363

364

## 366 References

- 1: Herring, S. C., Hoerling, M. P., Kossin, J. P., Peterson, T. C., & Stott, P. A., Explaining extreme events of 2014 from a climate perspective. *Bulletin of the American Meteorological Society*, **96**(12), S1-S172, 2015
- 2: Seneviratne, S. I., et al., Changes in climate extremes and their impacts on the natural physical environment.. *Managing the risks of extreme events and disasters to advance climate change adaptation: Special report of the Intergovernmental Panel on Climate Change*, 109-230, 2012
- 3: Bindoff, N.L., Stott, P.A., AchutaRao, K.M., Allen, M.R., Gillett, N., Gutzler, D., Hansingo, K., Hegerl, G., Hu, Y., Jain, S. and Mokhov, I.I., CH10: Detection and attribution of climate change: from global to regional, 2013
- 4: Hoegh-Guldberg and Coauthors, CH3: Impacts of 1.5°C global warming on natural and human systems, 2018
- 5: Taylor, K.E., R.J. Stouffer, G.A. Meehl, An Overview of CMIP5 and the experiment design. *Bull. Amer. Meteor. Soc.*, **93**, 485-498, 2012
- 6: Eyring, V., Bony, S., Meehl, G. A., Senior, C. A., Stevens, B., Stouffer, R. J., & Taylor, K. E., Overview of the Coupled Model Intercomparison Project Phase 6 (CMIP6) experimental design and organization. *Geoscientific Model Development (Online)*, **9**, LLNL-JRNL-736881, 2016
- 7: Guo, Y., A., Gasparrini, B. G. Armstrong and Coauthors, Heat wave and mortality: a multicountry, multicomunity study. *Environmental health perspectives*, **125**(8), 087006, 2017
- 8: Vogel, E., Donat, M. G., Alexander, L. V., Meinshausen, M., Ray, D. K., Karoly, D., Meinshausen, N. & Frieler, K., The effects of climate extremes on global agricultural yields. *ERL*, **14**(5), 054010, 2019

- 9: Zuo, J., Pullen, S., Palmer, J., et al., Impacts of heat waves and corresponding measures: a review. *Journal of Cleaner Production*, 1-12, 2015
- 10: Whan, K., Zscheischler, J., Orth, R., Shongwe, M., Rahimi, M., Asare, E. O., & Seneviratne, S. I., Impact of soil moisture on extreme maximum temperatures in Europe. *Weather and Climate Extremes*, **9**, 57-67, 2015
- 11: Milly, P. C. D. and Dunne, K. A., Potential evapotranspiration and continental drying. *Nature Clim. Ch.*, **6**, 946-949, 2016
- 12: Schär, C., P. L. Vidale, D. Lüthi, C. Frei, C. Häberli, M. A. Liniger and C. Appenzeller, The role of increasing temperature variability in European summer heatwaves. *Nature*, **427**, 332-336, 2004
- 13: Hersbach and Coauthors, Operational global reanalysis: progress, future directions and synergies with NWP. European Centre for Medium Range Weather Forecasts, 2018
- 14: Hanlon H., Hegerl, G.C., Tett, S.F.B., Smith, D. , Can a decadal forecasting system predict temperature extreme indices?. *J. Climate*, **26**, 3728-3744, 2013
- 15: Seneviratne, S.I., Corti, T., Davin, E.L., Hirschi, M., Jaeger, E.B., Lehner, I., Teuling, A.J., Investigating soil moisture–climate interactions in a changing climate: a review. *Earth-Sci. Rev.*, **99**(3), 125-161, 2010
- 16: Seneviratne, S. I., Wilhelm, M., Stanelle, T., van den Hurk, B., Hagemann, S., Berg, A., ... & Claussen, M., Impact of soil moisture-climate feedbacks on CMIP5 projections: First results from the GLACE-CMIP5 experiment. *Geophysical Research Letters*, **40**(19), 5212-5217, 2013
- 17: Miralles, D. G., Gentile, P., Seneviratne, S. I., & Teuling, A. J., Land–atmospheric feedbacks during droughts and heatwaves: state of the science and current challenges. *Annals of the New York Academy of Sciences*, **1436**(1), 19, 2019

- 18: Hall, A., Cox, P., Huntingford, C., & Klein, S. , Progressing emergent constraints on future climate change. *Nature Climate Change*, 2019
- 19: van Vuuren DP, JA Edmonds, M Kainuma, K Riahi, AM Thomson, K Hibbard, GC Hurtt, T Kram, V Krey, J-F Lamarque, T Masui, M Meinshausen, N Nakicenovic, SJ Smith, and S Rose, The representative concentration pathways: an overview *Climatic Change*. **109**(1-2), 5-31, 2011
- 20: Gidden, M., Riahi, K., Smith, S., Fujimori, S., Luderer, G., Kriegler, and Coauthors, Global emissions pathways under different socioeconomic scenarios for use in CMIP6: a dataset of harmonized emissions trajectories through the end of the century. *Geoscientific Model Development Discussions*, **12**(4), 1443-1475, 2019
- 21: King, A. D., Knutti, R., Uhe, P., Mitchell, D. M., Lewis, S. C., Arblaster, J. M., & Freychet, N., On the linearity of local and regional temperature changes from 1.5 C to 2 C of global warming. *Journal of Climate*, **31**(18), 7495-7514, 2018
- 22: Mitchell, Daniel, Krishna AchutaRao, I. Bethke, U. Beyerle, Andy Ciavarella, P. M. Forster, Jan Fuglestedt et al., Half a degree additional warming, prognosis and projected impacts (HAPPI): background and experimental design. *Geoscientific Model Development*, **10**, 571-583, 2017
- 23: Schurer, A. P., Cowtan, K., Hawkins, E., Mann, M. E., Scott, V., & Tett, S. F. B. , Interpretations of the Paris climate target. *Nature Geoscience*, **11**(4), 220, 2018
- 24: Li Z. and Z.-W. Yan, Homogenized daily mean/maximum/minimum temperature series for China from 1960-2008. *Atmospheric and Oceanic Science Letters*, **2**(4), 237-243, 2009
- 25: Cornes, R., G. van der Schrier, E.J.M. van den Besselaar, and P.D. Jones, An Ensemble Version of the E-OBS Temperature and Precipitation Datasets. *J. Geophys. Res. Atmos.*, **123**, 2018